Chinese Chemical Letters 35 (2024) 109341

Contents lists available at ScienceDirect

Chinese Chemical Letters

journal homepage: www.elsevier.com/locate/cclet

Fe-N-C heterogeneous Fenton-like catalyst for the degradation of tetracycline: Fe-N coordination and mechanism studies

Weichen Zhu[a], Wei Zuo[a,*], Pu Wang[a], Wei Zhan[a,*], Jun Zhang[a], Lipin Li[a], Yu Tian[a], Hong Qi[a], Rui Huang[b,c]

[a] State Key Laboratory of Urban Water Resource and Environment (SKLUWRE), School of Environment, Harbin Institute of Technology, Harbin 150090, China
[b] Guangdong Yuehai Water Investment Co., Ltd., Shenzhen 518021, China
[c] National Engineering Research Center of Urban Water Resources Co., Ltd., Harbin Institute of Technology, Harbin 150090, China

ARTICLE INFO

Article history:
Received 3 September 2023
Revised 7 November 2023
Accepted 23 November 2023
Available online 30 November 2023

Keywords:
H_2O_2 activation
Advanced oxidation process
Superoxide radicals
Degradation pathways
EXAFS

ABSTRACT

Fe-N-C materials have received increasing attention, due to its distinctive catalytic activity. However, the Fe-N coordination number dependence of catalytic ability and mechanism for H_2O_2 activation remain elusive. Herein, a series of Fe-N-C heterogeneous Fenton-like catalysts with different Fe-N coordination number were prepared for tetracycline degradation. The results demonstrated that samples with Fe-N_4 structure exhibited high activity. The excellent performance was mainly ascribed to the high adsorption capacity and the formation of superoxide radicals ($^{\bullet}O_2^-$) catalyzed by Fe linked to pyridinic nitrogen. The intermediates and degradation pathways of tetracycline degradation by Fe-N-C/H_2O_2 system were analyzed by liquid chromatography coupled to tandem mass spectrometry (LC-MS/MS). Furthermore, we applied our Fe-N-C catalysts to treat simulated pharmaceutical wastewater with high tetracycline degradation capacity despite high concentrations of organic matter such as oxalic acid and various ionic interferences. Our work reveals the dependence of the activation H_2O_2 on the Fe-N coordination environment and the degradation mechanism of these catalysts. It provides insights into the prospects for tuning the catalyst in practical applications.

Tetracyclines (TC) represent a prominent class of antibiotics with global significance, and their presence in surface and groundwater is noteworthy due to their chemical stability and resistance to biodegradation [1,2]. Notably, TC concentrations in hospital and pharmaceutical wastewater can reach exceptionally high levels, exceeding 100 mg/L in certain instances [3]. In response to the pressing need for effective removal of these persistent organics, advanced oxidation processes (AOPs) have been demonstrated as a highly efficient and green technologies by generating strong oxidizing free radicals [4–7]. Among the various AOPs, H_2O_2-based heterogeneous Fenton process using solid catalysts instead of Fe^{2+} have been fully developed [8]. Solid catalysts extend the pH operational range, while also minimizing chemical usage and sludge formation, effectively addressing the limitations of homogeneous Fenton systems [9–12]. Furthermore, the facile recovery and recyclability of these catalysts markedly diminish associated costs [13–17]. However, the performance of these heterogeneous Fenton catalysts depends on their specific surface area, active sites, and structural properties [18,19]. They still face some inherent problems of limited active sites, low H_2O_2 activation and difficulty in meeting the industrial requirements compared to the homogeneous Fenton process [20].

Single-atom catalysts (SACs), which combine the high activity of homogeneous catalysts with the easy recovery of heterogeneous catalysts, have emerged as a promising research area in the field of environmental catalysis [21,22]. By maximizing atom utilization, the catalyst activity and selectivity have also been greatly exploited [23]. Currently, single-atom transition metal-nitrogen-carbon (M-N-C, M = Fe, Ni, Mn, *etc.*) has been widely studied in oxygen reduction reaction (ORR) [24], hydrogen evolution reaction (HER) [25], and CO_2 reduction reaction (CO_2RR) [26], due to its distinctive catalytic activity. Previous studies have shown that M-N_x is the main active site affecting the catalytic reaction rate [27–30]. In recent years, it has been shown that the electron spin state can be effectively optimized by changing the coordination number of Fe-N_x, which in turn affects the catalytic activity [31]. It was also reported that carbon nanotube-based catalysts with five Co-N coordination numbers performed significantly better than the four-nitrogen

* Corresponding authors.
E-mail addresses: zuoweistar@163.com (W. Zuo), hitzhanwei@hit.edu.cn (W. Zhan).

https://doi.org/10.1016/j.cclet.2023.109341
1001-8417/

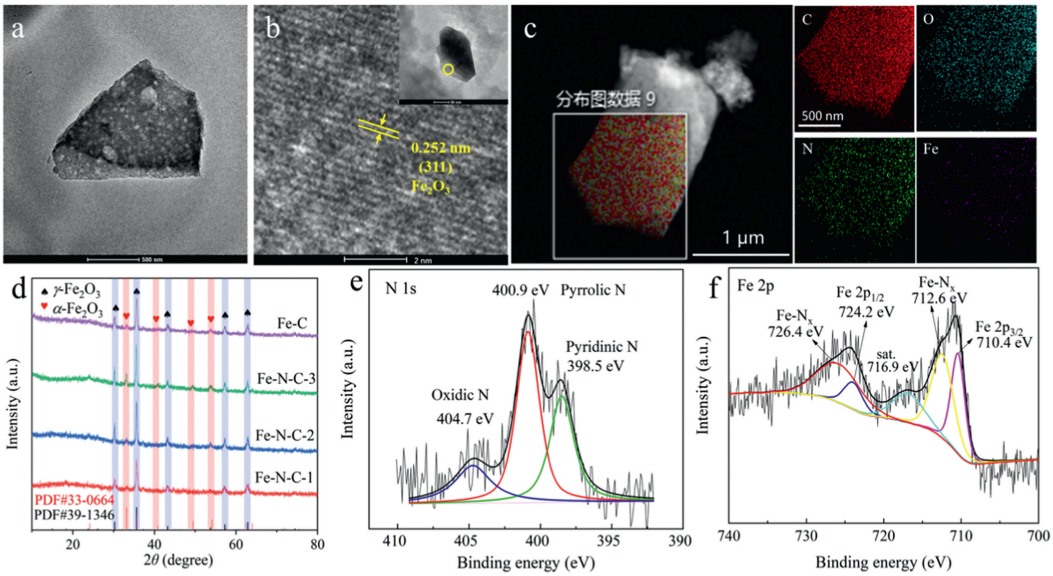

Fig. 1. (a) TEM image of Fe-N-C-2. (b) HRTEM image of nanoparticle region marked by yellow circle of Fe-N-C-2 (inset figure: TEM image of the nanoparticle). (c) TEM and EDS mapping images of Fe-N-C-2 with uniform distribution of Fe, C, N, and O. (d) XRD patterns of various Fe-N-C catalysts (inset of standard peaks of Fe_2O_3). (e, f) XPS spectra of different elements present in the Fe-N-C-2: (e) N 1s and (f) Fe 2p.

coordination case prepared by the same method [32]. Based on the interaction of light and adsorbed O_2, g-C_3N_4 anchored with Ti single atoms could be converted from Ti-N_6 to Ti-N_4, prompting a rapid generation of clean active substances [33]. Nevertheless, research on the effect of coordination number of Fe-N-C and its degradation mechanism are still unclear [34–36].

In this study, a series of heterogeneous Fenton-like catalysts with Fe-N-C structures were prepared by a two-step pyrolysis method (Fig. S1 in supporting information). The Fe-N coordination number could be conveniently tuned by adjusting the amount of nitrogen source using this method. The differences in the performance of Fe-N-C catalysts affected by Fe-N coordination number in H_2O_2-based Fenton systems were investigated using TC as the target contaminant. Subsequently, the adsorption, major radicals, possible degradation mechanisms and pathways within the studied systems were explored. This study unveils the coordination-dependent activity behavior and mechanism of heterogeneous Fenton-like catalyst, which lays the foundation for the design of non-precious Fe-N-C catalyst.

The prepared catalysts were labeled as Fe-N-C-1, Fe-N-C-2, Fe-N-C-3 and Fe-C by the difference in the amount of Fe added (Text S1 in Supporting information). The scanning electron microscopy (SEM) images (Figs. S2a-h in Supporting information) reveal that the amounts of irregular particles adhered to the catalyst surface elevated with an increase in the Fe ratio. It can also be observed from the Fig. S3 (Supporting information) that the particles were mainly composed of Fe and O, while the C and N elements were uniformly distributed on the surface of the catalyst. The transmission electron microscope (TEM) image (Fig. 1a) shows that obvious nanoparticles were evenly distributed on the catalyst. Moreover, high resolution transmission electron microscope (HRTEM) characterizations (Fig. 1b) demonstrate that the lattice fringe spacing of the nanoparticle was 0.252 nm, which could be correspond well to (311) crystallographic plane of Fe_2O_3 [37]. In addition, the TEM-energy-dispersive X-ray spectroscopy (TEM-EDS) scan in Fig. S4 (Supporting information) reveals that the ratio of Fe to O in the nanoparticles was 2:3, which partly confirmed the presence of Fe_2O_3. Conversely, the EDS scans of the region without nanoparticles (Fig. 1c) demonstrate that the four elements (C, N, O, and Fe) were uniformly distributed in Fe-N-C-2. The Fe content of Fe-N-C-2 was determined to be 16.4 wt% by Inductively Coupled Plasma Optical Emission Spectrometer (ICP-OES). Table S1 (Supporting information) shows weight percentage of the elements in different regions. In the region without nanoparticles, the weight percentages of Fe and N were 1.46% and 6.83%, respectively. This Fe mass fraction of 1.46% was close to the Fe content reported in other studies involving Fe-SACs [38,39]. These results indicate that N, and Fe atoms were successfully integrated into the C framework. Therefore, it can be speculated that Fe-N-C catalysts comprises both Fe_2O_3 nanoparticles and atomically dispersed Fe.

The crystal structures of the catalysts were further investigated using X-ray Diffractometer (XRD). As depicted in Fig. 1d, all studied samples exhibited characteristic peaks corresponding to the cubic γ-Fe_2O_3 crystalline phases. The presence of N contributed to a higher degree of crystallinity of γ-Fe_2O_3. It is noteworthy that the crystallinity increased gradually with the increase of Fe injection, and the addition of Fe beyond a certain point led to the formation of α-Fe_2O_3. These Fe_2O_3 provide the magnetism for the catalyst to be recovered (Text S2 and Fig. S5 in Supporting information). X-ray Photoelectron Spectroscopy (XPS) was carried out to analyze the valence states and the chemical bond among the elements of the catalyst. As shown in Fig. S6 (Supporting information), the existence of C-N and O-Fe in the Fe-N-C-2 catalyst were confirmed [40]. The corresponding fine-scan N 1s XPS spectrum (Fig. 1e) could be nicely deconvoluted into three component peaks, which were pyridinic N (398.5 eV), pyrrolic N (400.9 eV), and oxidized N (404.7 eV) [41,42]. Furthermore, Fe $2p_{3/2}$ and Fe $2p_{1/2}$ exhibited two peaks at 710.4 eV and 724.2 eV, respectively, indicating the +3-valence of Fe (Fig. 1f). The peaks at 712.6 eV and 726.4 eV belonged to the Fe-N_x configuration.

The presence of Fe-N bonds was further confirmed by the Fourier transform (FT) k^3-weighted extended X-ray absorption fine structure (EXAFS) in Fig. 2a. The distinct peaks of Fe-N-C samples at 1.5 Å corresponded to the Fe-N and Fe-O bonds, which markedly different from Fe foil. The curve fit and fitting results reveal that the first shell Fe-N coordination numbers of Fe-N-C-1, Fe-N-C-2 and Fe-N-C-3 were determined as 3.3, 3.8 and 4.1, respectively (Figs. 2b–d, Fig. S7 and Tables S2-S4 in Supporting information). The Wavelet Transform (WT) of EXAFS could visualize the types of coordination atoms while demonstrating the radial distances. The

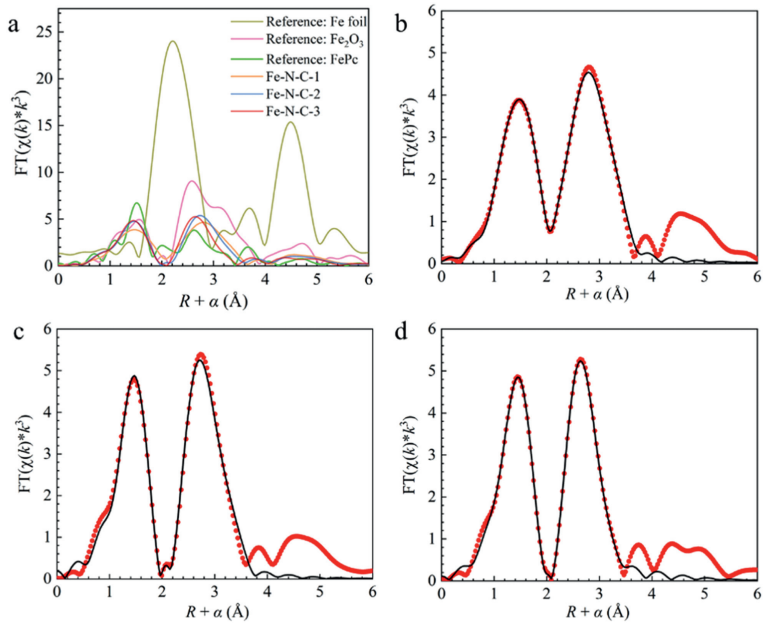

Fig. 2. (a) *R* space of the k^3-weighted Fe K-edge EXAFS spectra of Fe-N-C samples with the references. (b-d) Fe K-edge EXAFS (points) and curve fit (line) for (b) Fe-N-C-1, (c) Fe-N-C-2 and (d) Fe-N-C-3, shown in *R* space (FT magnitude). The data are k^3-weighted and not phase-corrected.

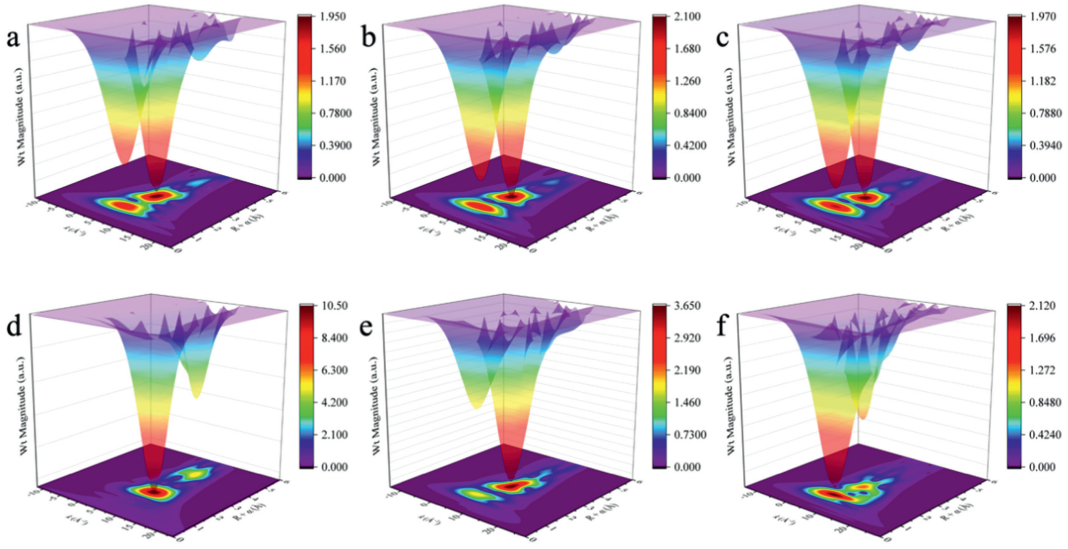

Fig. 3. WT spectrum of the k^3-weighted EXAFS (a-Fe-N-C-1, b-Fe-N-C-2, c-Fe-N-C-3, d-Fe foil, e-Fe_2O_3, f-FePc).

WT spectrum of Fe-N-C samples (Figs. 3a–c) exhibited two contour intensities at 5.2 $Å^{-1}$ and 6.6 $Å^{-1}$, which matched with FePc and Fe_2O_3 but significantly different from Fe foil (Figs. 3d-f), indicating the existence of the Fe-N and Fe-O bonds. Moreover, the intensity of the Fe-N peak increased with the higher Fe-N ratio, which indicated that the Fe-N coordination number enhanced with the increase of Fe dosage.

The Fe-N-C samples obtained in this study were assessed for their ability to activate H_2O_2 for TC degradation. As shown in Fig. 4a, Fe-N-C-3 showed a stronger adsorption capacity for TC during adsorption stage, potentially due to its larger specific surface area and more adsorption sites (Text S3, Figs. S8 and S9, and Table S5 in Supporting information). After the H_2O_2 was added, TC was rapidly degraded within 30 min and the concentration reached equilibrium. Within 120 min, Fe-N-C-1, Fe-N-C-2, Fe-N-C-3, Fe-C, γ-Fe_2O_3 and α-Fe_2O_3 could achieve 85.20%, 89.13%, 88.29%, 60.00%, 40.64% and 9.30% removal respectively. Notably, the degradation efficiency of the Fe-N-C samples was significantly improved compared with the commercial Fe_2O_3, indicating that the γ-Fe_2O_3 and α-Fe_2O_3 present in the catalysts were not the primary active components. The catalytic performance of Fe-C was remarkably inferior to that of Fe-N-C-2 with the same Fe dosage, demonstrating that the crucial role of N in the catalyst. Furthermore, the degradation performance increased as the coordination number increased from 3.3 to 3.8, while there was no significant difference in performance around 4. It should be noted that the coordination number here is an average value, which means that the coordination number is dominated by 3 with a small amount of higher coordination number catalysts when $x = 3.3$, while the coordination number is dominated by 4 when $x = 3.8$ or 4.1. Thus, this result suggests that the degradation at coordination number 4 is better than that at 3. Changes in nitrogen coordination number could alter the electronic structure of the catalyst surface, thus affecting the adsorption and reaction processes of reactants on the catalyst surface [43]. As the

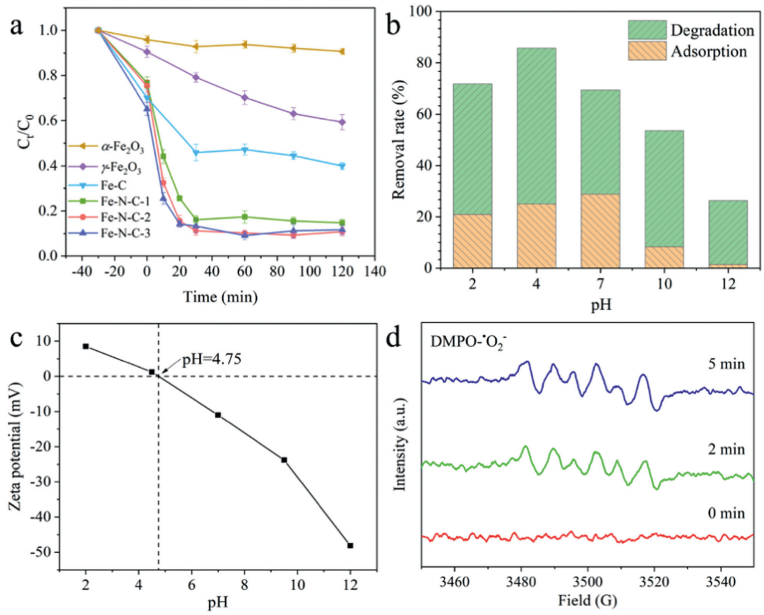

Fig. 4. (a) The removal of TC in different reaction systems. (b) Effects of pH on the removal of TC by Fe-N-C-2 at pH 2, 4.5, 7, 9.5, and 12, respectively. (c) Zeta potential analysis of Fe-N-C-2. (d) EPR signals of DMPO-$^{\bullet}O_2^-$. Reaction conditions: [TC] = 10 mg/L, [catalysts] = 0.2 g/L, [H_2O_2] = 20 mmol/L, initial pH 4.0 ± 0.1 and at room temperature, if not otherwise specialized.

nitrogen coordination number gradually increases from 3 to 4, the interaction between the active site and H_2O_2 increased, while the energy barrier during the reaction process decreased [44]. Table S6 (Supporting information) presents a comparative assessment of catalysts employed in the activation of H_2O_2 for TC degradation. Notably, the Fe-N-C catalyst demonstrates enhanced TC degradation efficacy under comparable experimental conditions. Otherwise, the Fe leaching concentration in the Fe-N-C-2/H_2O_2 system was 0.072 mg/L, and it was experimentally demonstrated that the homogeneous Fenton reaction of Fe ions at this concentration had little effect on the degradation efficiency (Fig. S10 in Supporting information). Thus, the TC degradation mechanism part of this study mainly explored the heterogeneous degradation process of Fe-N-C.

The variation of the degradation effect of Fe-N-C-2 catalysts on TC under different pH conditions and the influence of different coexisting ions was also investigated (Fig. S11 in Supporting information). The results show that the highest catalytic degradation efficiency was achieved at around pH 4. Moreover, among the tested ions, HCO_3^- and $H_2PO_4^-$ exhibited the most significant influence on the TC degradation process due to its reaction with H_2O_2 and Fe ions. The optimal conditions were determined as a H_2O_2 concentration of 10 mmol/L and pH 4. These conditions were subsequently utilized to investigate the degradation mechanism.

Adsorption is a crucial step for heterogeneous Fenton-like catalysts to degrade pollutants, wherein the pollutants are concentrated at the interface with the highest concentration of active free radicals. It has been reported that the adsorption between contaminants and materials mainly originates from electrostatic interactions, electron-donor-acceptor interactions (π-π EDA) and hydrogen-bonding (H-bonding) interactions [45], where electrostatic and hydrogen-bonding interactions are susceptible to pH effects. Fig. 4b shows the adsorption proportion of Fe-N-C-2 catalyst for TC removal at different pH. As the pH increased from 2 to 7, the adsorption rate increased from 20.94% to 28.83%. However, as the pH continued to increase, the adsorption performance of the catalyst significantly decreased. The results of zeta potential analysis (Fig. 4c) show that when pH was < 4.75, the Fe-N-C-2 catalyst carried a positive charge, while when pH > 4.75, it carried a negative charge. In addition, the chemical structure and ionization equilibrium of TC were shown in Fig. S12 (Supporting information). When the solution pH < 3.3, TC mainly existed in the form of TCH_3^+, which exhibited electrostatic repulsion with the Fe-N-C catalyst. When 7.7 > pH > 3.3, TC mainly existed as TCH_2, and the electrostatic repulsion was weakened. However, when the pH > 7.7 or 9.7 > pH > 7.7, TC partially or completely deprotonated to form TCH^- and TC_2^-, resulting in a significant increase in repulsion force. Therefore, the repulsion between TC and Fe-N-C catalyst was weak under acidic conditions and strong under alkaline conditions. It is worth noting that at pH 4, both the adsorption and degradation effects can achieve relatively optimal states for the catalyst, and the adsorption effect plays a relatively important role in this degradation process.

To investigate the main reactive species responsible for the degradation of TC, three quenchers, namely isopropyl alcohol, *p*-benzoquinone and furfuryl alcohol, were employed to selectively capture hydroxyl radical ($^{\bullet}OH$), superoxide radical ($^{\bullet}O_2^-$) and singlet oxygen capture ($^1O_2$), respectively [46]. Figs. S13a, b and d (Supporting information) show that the addition of $^{\bullet}OH$ and $^1O_2$ quenchers did not significantly affect the degradation of TC. However, in the presence of $^{\bullet}O_2^-$ quencher, it could be observed that the TC concentration increased, indicating the TC desorbed from the catalyst and was not degraded (Figs. S13a and c in Supporting information). Furthermore, the electron paramagnetic resonance (EPR) results (Fig. 4d, Figs. S13e and f in Supporting information) show that only signals of $^{\bullet}O_2^-$ was detected in the first 2 min, while the signals did not continue to increase in the next 3 min. Meanwhile, no signal of $^{\bullet}OH$ and $^1O_2$ was observed in the system. Thus, $^{\bullet}O_2^-$ plays a key role in the catalytic reaction.

The active site on Fe-N-C-2 was investigated by analyzing changes in XPS spectra of the catalyst before and after the Fenton-like reaction (Figs. S14, S15 and Table S7 in Supporting information). As shown in Figs. S15a-c (Supporting information), the results reveal that part of the graphitic phase of carbon (C–C) was oxidized by H_2O_2 or $^{\bullet}O_2^-$ during the catalytic degradation process, which increased the oxygen-containing groups on the catalyst surface and also led to the decrease of the peak area ratios of O–H and O-Fe and the decrease of the elemental C share. For

the N 1s spectra (Fig. S15b in Supporting information), the content of the N–O and pyridinic N decreased, but the percentage of pyrrolic N peak area increased from 52.99% to 59.09%. It is noteworthy that pyridinic N, which is nitrogen attached between two carbon atoms on the edge of graphitic carbon with a lone pair of electrons, is chemically more reactive than pyrrolic N, which has two p-electrons and π-bonds conjugated [47]. For the Fe 2p spectra (Fig. S15d in Supporting information), both peak areas of Fe-N_x showed a decreasing trend from 24.93% and 29.81% to 21.37% and 24.18%, respectively, while both peak areas of Fe 2p showed an increasing trend. Since there was a decrease in the catalytic activity after degradation (Fig. S16 in Supporting information), it could be inferred that the Fe connected with pyridinic N might be the main catalytic active site.

The cyclic degradation experiments demonstrated a gradual decrease in catalyst performance over multiple cycles (Fig. S16). Chemical stability assessment showed that only 0.02% of Fe leached into the reaction solution after the degradation process, indicating limited Fe dissolution. Additionally, XPS analysis revealed the conversion of pyridinic N-Fe to pyrrolic N and Fe(III) might also be the main factor for the gradual weakening of catalytic activity.

Therefore, combining the above analysis results and existing studies, it is assumed that the degradation mechanism of the catalyst was shown in Fig. S17 (Supporting information). The process of TC removal by Fe-N-C-2 is as follows: firstly, the catalyst adsorbed and immobilized TC on the catalyst surface by π-π EDA, electrostatic interaction, etc. Subsequently, pyridinic N-linked Fe activated H_2O_2 to produce $^{\bullet}O_2^-$, which decomposed TC into intermediate products. And then, the intermediate products gradually mineralized into small molecules such as CO_2 and H_2O to achieve efficient and green removal of the target pollutants.

The absorption spectra of TC degradation by Fe-N-C-2 were analyzed using UV–vis spectroscopy (Fig. S18a in Supporting information). The results show that after the addition of H_2O_2, the intensity of the peaks at 357 nm and 276 nm gradually decreased over time, and the characteristic peaks disappeared, suggesting that the Fenton-like reaction destroyed the aromatic nucleus of TC and its intermediates [48]. The TOC degradation effect of Fe-N-C-2 degradation process was used to demonstrate the mineralization level of the process, and the TOC removal rate at 60 min was 16.39% (Fig. S18b in Supporting information). In order to further identify the intermediates and degradation pathways of TC by Fe-N-C/H_2O_2 system, liquid chromatography coupled to tandem mass spectrometry (LC-MS/MS) was used for the characterization in positive mode. A total of twelve intermediates were tentatively identified, with their structures and chemical formulas summarized in Table S8 (Supporting information) and the mass spectra shown in Fig. S19 (Supporting information). Fig. 5 demonstrates the proposed TC degradation pathways based on the intermediates. In pathway I, the *N*,*N*-dimethylamine of TC undergoes oxidative rupture to yield **P1** (*m/z* 431), which is followed by oxidative dehydrogenation to produce **P2** (*m/z* 429). In pathway II, the "D" ring of TC is first oxidatively hydroxylated to **P3** (*m/z* 461), which is further oxidatively dehydrogenated to **P4** (*m/z* 459) or hydroxylated to **P5** (*m/z* 477). **P6** (*m/z* 417) is formed from the oxidative ring opening reaction,

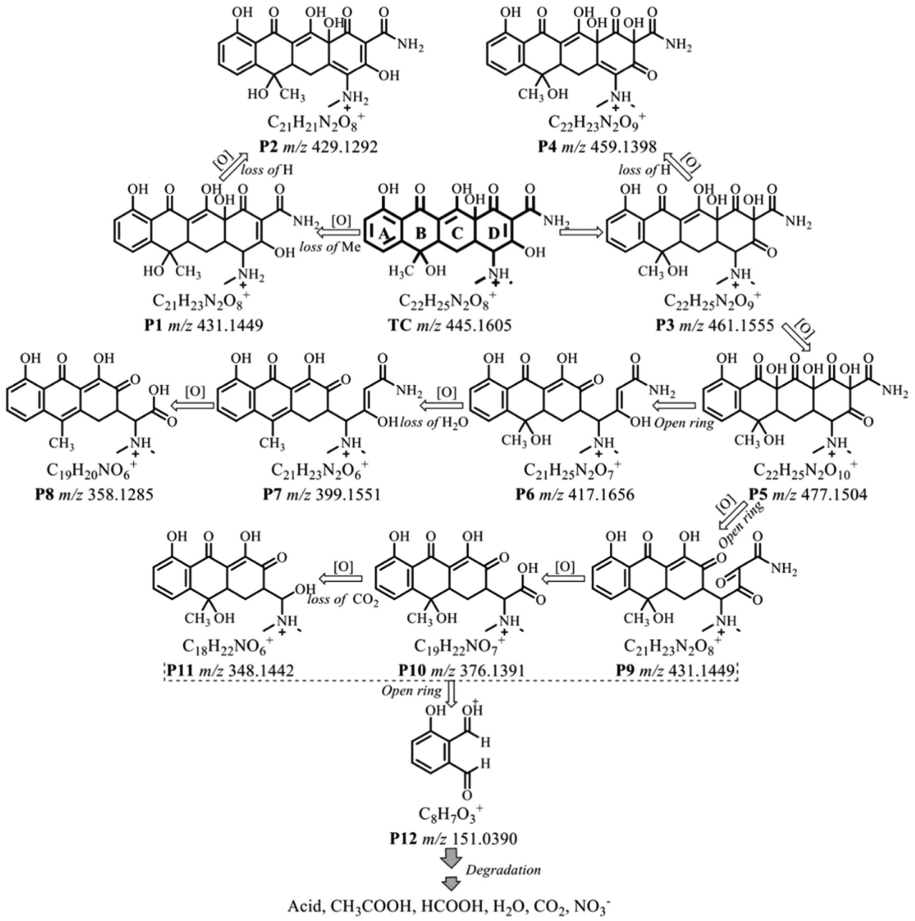

Fig. 5. Possible pathways proposed for TC degradation in Fe-N-C/H_2O_2 system. Chromatographic separation conditions: Eclipse Plus C18 (100 mm × 4.6 mm, 3.5 μm) at a flow rate of 0.35 mL/min, mobile phase (a mixture of acetonitrile/water (0.1% formic acid)) and injection volume = 10 μL. Mass spectrometry conditions: positive mode and the spray voltage of 3.8 kV.

and then be dehydrated to yield **P7** (*m/z* 399). **P7** is further undergoes to form **P8** (*m/z* 358) by oxidative removal of the side chain. In pathway III, **P9** (*m/z* 431) is transformed from **P5** through oxidation of the "D" ring. Then, **P10** (*m/z* 376) is generated from **P9** after the attack of the side chain, and subsequently decarboxylated to undergo oxidative hydroxylation to form **P11** (*m/z* 348). Further transformation of these intermediates in the Fe-N-C/H_2O_2 system generates **P12** (*m/z* 151), which in turn forms smaller molecular species and eventually H_2O, CO_2, NO_3^- and NH_4^+. The intermediates were not fully mineralized within 60 min, which explains the residual TOC after the treatment.

Finally, pharmaceutical simulated wastewater with high concentrations of organic matter and various ionic interferences was used to investigate the application of Fe-N-C catalyst (Text S4, Table S9, Figs. S20 and S21 in Supporting information). The results reveal that the removal rate of TC and TOC reached 70.49% and 35.97% at 540 min, suggesting the strong interference resistance of Fe-N-C/H_2O_2 system.

In summary, we studied the effects of Fe-N coordination number on the catalyst structure, as well as the degradation performance and possible mechanism of Fe-N-C samples. The EXAFS analysis revealed that the first shell Fe-N coordination numbers of Fe-N-C-1, Fe-N-C-2 and Fe-N-C-3 were determined as 3.3, 3.8 and 4.1, respectively. During the H_2O_2 activated process, the results showed that the degradation efficiency at coordination number 4 was better than 3. The EPR analysis demonstrated that $^{\bullet}O_2^-$ played a key role as major reactive species in the catalytic reaction. By comparing the XPS energy spectra of Fe-N-C-2 before and after use, it was inferred that the Fe linked to pyridine nitrogen might be the catalytic active site of this material. This work presents the correlation between the Fe-N coordination number and catalytic activity, and demonstrates the possible mechanism and degradation pathways of these catalysts, establishing a foundation for the design and application of Fe-N-C catalysts.

Declaration of competing interest

The authors declare that they have no known competing financial interests or personal relationships that could have appeared to influence the work reported in this paper.

Acknowledgments

This work was supported by the National Key Research and Development Program of China (No. 2019YFC1906401-03) and the Harbin Institute of Technology National Engineering Research Center of Urban Water Resources Co., Ltd. (No. GJS-YF-LX202207280002).

Supplementary materials

Supplementary material associated with this article can be found, in the online version, at doi:10.1016/j.cclet.2023.109341.

References

[1] Y. Hong, C. Li, B. Yin, et al., Chem. Eng. J. 338 (2018) 137–146.
[2] Y. Zhang, J. Zhou, X. Chen, L. Wang, W. Cai, Chem. Eng. J. 369 (2019) 745–757.
[3] X.R. Jing, Y.Y. Wang, W.J. Liu, Y.K. Wang, H. Jiang, Chem. Eng. J. 248 (2014) 168–174.
[4] G. Boczkaj, A. Fernandes, Chem. Eng. J. 320 (2017) 608–633.
[5] I. Casero, D. Sicilia, S. Rubio, D. Pérez-Bendito, Water Res. 31 (1997) 1985–1995.
[6] M.I. Stefan (Ed.), Advanced Oxidation Processes for Water Treatment: Fundamentals and Applications, IWA Publishing, London, 2017.
[7] K. Qian, H. Chen, W. Li, et al., Environ. Sci. Technol. 55 (2021) 7034–7043.
[8] M. Cheng, C. Lai, Y. Liu, et al., Coord. Chem. Rev. 368 (2018) 80–92.
[9] A.D. Bokare, W. Choi, J. Hazard. Mater. 275 (2014) 121–135.
[10] J. Wang, R. Zhuan, Sci. Total Environ. 701 (2020) 135023.
[11] J. Wang, J. Tang, Chemosphere 276 (2021) 130177.
[12] H. Peng, W. Xiong, Z. Yang, et al., Chem. Eng. J. 457 (2023) 141317.
[13] E.G. Garrido-Ramírez, B.K.G. Theng, M.L. Mora, Appl. Clay Sci. 47 (2010) 182–192.
[14] S. Navalon, A. Dhakshinamoorthy, M. Alvaro, H. Garcia, ChemSusChem 4 (2011) 1712–1730.
[15] C. Tang, M. Cheng, C. Lai, et al., J. Environ. Chem. Eng. 11 (2023) 110395.
[16] C. Guo, M. Cheng, G. Zhang, et al., Environ. Sci.: Nano 10 (2023) 1528–1552.
[17] Q. Shi, S. Pu, X. Yang, et al., Chin. Chem. Lett. 33 (2022) 2129–2133.
[18] J. Xu, X. Zheng, Z. Feng, et al., Nat. Sustain. 4 (2021) 233–241.
[19] H. Cao, J. Wang, J.H. Kim, et al., Appl. Catal. B 296 (2021) 120362.
[20] Y. Yin, W. Li, C. Xu, et al., Environ. Sci.: Nano 7 (2020) 2595–2606.
[21] F. Chen, X. Jiang, L. Zhang, R. Lang, B. Qiao, Chin. J. Catal. 39 (2018) 893–898.
[22] A. Wang, J. Li, T. Zhang, Nat. Rev. Chem. 2 (2018) 65–81.
[23] Z. Li, S. Ji, Y. Liu, et al., Chem. Rev. 120 (2019) 623–682.
[24] X. Chen, N. Wang, K. Shen, et al., ACS Appl. Mater. Interfaces 11 (2019) 25976–25985.
[25] W. Chen, J. Pei, C.T. He, et al., Adv. Mater. 30 (2018) 1800396.
[26] B. Chen, B. Li, Z. Tian, et al., Adv. Energy Mater. 11 (2021) 2102152.
[27] Y. Li, X. Liu, L. Zheng, et al., J. Mater. Chem. A: Mater. 7 (2019) 26147–26153.
[28] X. Li, C.S. Cao, S.F. Hung, et al., Chem 6 (2020) 3440–3454.
[29] J. Li, S. Hu, Y. Li, et al., Carbon 206 (2023) 62–71.
[30] C. Zhou, Y. Liang, W. Xia, et al., J. Hazard. Mater. 441 (2023) 129871.
[31] D. Xue, P. Yuan, S. Jiang, et al., Nano Energy 105 (2023) 108020.
[32] M. Xie, M. Yao, S. Zhang, et al., Sep. Purif. Technol. 304 (2023) 122398.
[33] Z. Hu, Y. Zhang, L. Pu, et al., J. Clean. Prod. 377 (2022) 134423.
[34] B. Huang, Z. Wu, H. Zhou, et al., J. Hazard. Mater. 412 (2021) 125253.
[35] Z. Miao, X. Wang, Z. Zhao, et al., Adv. Mater. 33 (2021) 2006613.
[36] Q. Ma, H. Jin, J. Zhu, et al., Adv. Sci. 8 (2021) 2102209.
[37] D. Cao, H. Li, L. Pan, et al., Sci. Rep. 6 (2016) 1–9.
[38] X.F. Yang, A. Wang, B. Qiao, et al., Acc. Chem. Res. 46 (2013) 1740–1748.
[39] M. Yang, R. Wu, S. Cao, et al., Chem. Eng. J. 451 (2023) 138606.
[40] C. Tang, B. Wang, H.F. Wang, Q. Zhang, Adv. Mater. 29 (2017) 1703185.
[41] W. Hu, C. Wang, H. Tan, et al., Nat. Commun. 12 (2021) 1854.
[42] J. Ma, L. Xu, C. Shen, et al., Environ. Sci. Technol. 52 (2018) 3608–3614.
[43] J. Wang, B. Li, Y. Li, et al., Adv. Sci. 8 (2021) 2101824.
[44] H. Fu, J. Wei, G. Chen, et al., Appl. Catal. B 321 (2023) 122012.
[45] C.A. Hunter, K.R. Lawson, J. Perkins, C.J. Urch, Perkin Trans. 2 (2001) 651–669.
[46] I. Michael-Kordatou, M. Iacovou, Z. Frontistis, et al., Water Res. 85 (2015) 346–358.
[47] Y. Zhao, J. Wan, H. Yao, et al., Nat. Chem. 10 (2018) 924–931.
[48] Y. Wang, H. Zhang, J. Zhang, et al., J. Hazard. Mater. 192 (2011) 35–43.